

# Molecular dynamics study of deformation and fracture for pure and bismuth-segregated tilt copper bicrystals

Fu-xin Zhou

Laboratory for Nonlinear Mechanics, Institute of Mechanics, Academia Sinica 100080, Beijing, People's Republic of China

Ba-yi Peng and Xi-jun Wu

Institute of Solid State Physics, Academia Sinica 230031, Hefei, People's Republic of China

(Received 22 September 1989; accepted for publication 2 April 1990)

The microprocess of deformation and fracture for pure and Bi-segregated  $\Sigma 3(\bar{1}\bar{1}1)/[101]$   $70.53^\circ$  and  $\Sigma 33(\bar{5}\bar{4}5)/[101]$   $58.99^\circ$  tilt bicrystals of metal copper has been studied by the molecular dynamics method. It has been found that deformation and fracture are dependent on the grain boundary (GB) structure and bismuth segregation. For pure  $\Sigma 33$  bicrystal, the deformation is mainly due to the glide of partial dislocations generated from the GB structural units where the GB dislocations exist. The ductile fracture is attributed to the dislocation emission, which leads to vacancy generation and void coalescence. The bismuth segregation weakens the atomic bonds between copper atoms in the vicinity of GB. Under the action of the external load, the weakened bonds break and lead to formation of microcracks. Finally, the brittle fracture takes place along the binding weakening region. For  $\Sigma 3$  bicrystal, the ductile fracture is related to the void coalescence generated not by dislocation emission but by lattice distortion, and the brittle fracture induced by bismuth segregation is also caused by the breaking of weakened Cu—Cu bonds.

## I. INTRODUCTION

Many experiments<sup>1-6</sup> indicated that grain boundary embrittlement (GBE) for metal copper could be caused by bismuth segregation, even for the case of bismuth in amounts as low as 0.002 wt. %. The GBE induced by bismuth segregation exhibited that the fracture is intergranular, and the fracture stress is strongly dependent on both the bismuth content and the grain boundary (GB) structure. Wu *et al.*<sup>7</sup> have studied the effect of bismuth segregation on chemical bonds of the GB for metal copper using the  $X\alpha$  discrete variational method. The results showed that the segregated bismuth atoms draw the electron charge from neighboring copper atoms in the vicinity of GB onto themselves and weaken the chemical bonds between those copper atoms. This result gave an understanding of the GBE from the electronic aspect. But the details of deformation and fracture for Bi-segregated copper bicrystals are still deficient. The aim of this work is to study the microprocess of deformation and fracture for pure and Bi-segregated tilt copper bicrystals for further understanding the GBE from the atomistic aspect. For interpreting the GBE of metals caused by impurity segregation, Chang *et al.*<sup>8</sup> and Ishida *et al.*<sup>9</sup> have studied the GBE of metal copper segregated by antimony and metal iron segregated by phosphorus using the Monte Carlo and molecular dynamics (MD) methods, respectively. In the case of Cu—Sb alloy, the results showed that under a uniaxial strain the weakened copper atomic bonds become the sources of microcracks and aggravate brittle fracture along the Sb-segregated GB. In the case of Fe—P alloy, it was found that the phosphorus segregation causes weakening of binding forces between the unit prism structure occurring in the GBs and the surrounding iron atoms, which results

in the crack propagation under an external load. In their studies the pair potentials, i.e., the Johnson potential and Morse potential, were adopted to describe atomic interactions. But pair potentials are only valid in cases where the atoms are contained in a definable volume. Hence, it is not reasonable to employ the pair-wise interactions in studying the fracture process during which new surfaces are formed. Furthermore, the details of generation and emission of the dislocation related to the deformation and fracture for Cu—Sb and Fe—P alloys have not been given. However, it is necessary to understand the GBE from the dislocation generation and emission aspect as well as from the bond-weakening aspect. Recently, Baskes *et al.*<sup>10</sup> have studied the fracture of the tilt GB for nickel and Ni<sub>3</sub>Al alloy using the MD method and employing the embedded atom method (EAM),<sup>11,12</sup> which provides a simple but accurate method of evaluating the energy and force in an ensemble of atoms and overcomes the deficiency of calculations employed in pair-wise interactions. They found that the fracture mechanism in metal nickel is related to secondary cracking, while in Ni<sub>3</sub>Al it is not. However, little is known about dislocation generation and emission.

In this paper, we study the microprocess of deformation and fracture for pure and bismuth-segregated tilt bicrystals of copper using the MD method with the atoms interacting via the empirical  $N$ -body potential proposed by Finnis and Sinclair,<sup>13</sup> which is a version of the EAM. The dislocation generation and emission are considered.

## II. COMPUTATIONAL PROCEDURE

As fracture is a volume-dependent process with the formation of new surfaces, in this work the empirical  $N$ -body potential for Cu—Cu atoms constructed by Ackland *et al.*<sup>14</sup> and the approximate  $N$ -body potentials for Cu—Bi

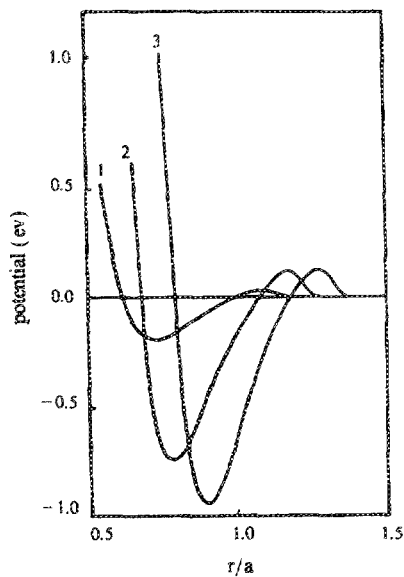


FIG. 1. The effective pair potentials for Cu—Cu (1), Cu—Bi (2) and Bi—Bi (3) (where  $a$  is the lattice constant of copper).

and Bi—Bi atoms constructed by Maeda *et al.*<sup>15</sup> are used. The effective pair potentials are plotted in Fig. 1.

To study the dependence of deformation and fracture on the GB structure, two different symmetric tilt bicrystals are considered: one containing the low  $\Sigma$  GB,  $\Sigma 3(\bar{1}\bar{1}1)/[101]$   $70.53^\circ$ , the other containing the high  $\Sigma$  GB,  $\Sigma 33(\bar{5}\bar{4}5)/[101]$   $58.99^\circ$ . The computational cell is chosen to be a bicrystal with the symmetric tilt GB at the center and is composed of two regions: regions I and II, as shown in Fig. 2. The GB plane is denoted by dashed lines in the  $Y$ - $Z$  plane. The tilt axis  $[101]$  is along the  $Z$  direction. Periodic border conditions are employed along the  $Y$  and  $Z$  directions. In general, it is required that the dimensions of the computational cell be chosen to be twice as large as the cutoff of the potential function. We consider only two atomic layers along the tilt axis, the dimension is twice as small as the cutoff. By evaluating the interaction between the periodic image atoms outside computational cell and the atoms inside the cell, the distance between them is smaller than the cutoff of the potential function. The effect of the atoms outside the computational cell on those inside has been already taken into account periodically. Other physical quantities such as pressure and energy are modified correspondingly. The reliability of such consideration has been demonstrated by the MD simulation of the re-

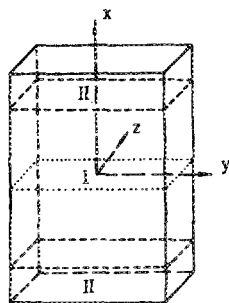


FIG. 2. The computational cell. Along the  $Y$ ,  $Z$  directions periodic border conditions are employed.

laxed structure of the  $\Sigma 5(310)/[100]$   $36.8^\circ$  symmetric tilt boundary.<sup>16</sup> In that study, two types of computational cells with six and two (100) atomic layers along the tilt axis were considered. The size in the former case was twice as large as the cutoff and that in the latter was smaller, but both gave the same result. Therefore, in the present study the consideration of two atomic layers along the tilt axis is reasonable and can save computational time. For the case of the  $\Sigma 3$  bicrystal, five  $\Sigma 3$  CSL periods in the  $Y$  direction and 490 atoms are taken into account. In the case of the  $\Sigma 33$  bicrystal, one  $\Sigma 33$  CSL period and 484 atoms are considered. As indicated by Hondros and McLean,<sup>2</sup> impurity segregation is mainly confined to within the first few atomic planes of GB. Computer studies<sup>17,18</sup> also indicated that the impurity bismuth atoms tend to segregate at a few atomic layers in the copper boundary. Using the polyhedral model, Pond *et al.*<sup>19</sup> have pointed out that the impurity atoms will replace the solvent atoms as substitutional atoms at GB, if the size of impurity atoms is larger than that of solvent atoms. For example, Chang *et al.*<sup>8</sup> described the impurity Sb atoms located at the substitutional lattice positions in copper GB. Therefore we assumed that bismuth atoms replace copper atoms at the vertexes of polyhedra in the GBs, such as octahedra and pentagonal bipyramid, as shown in Figs. 3(c) and 3(d). Thus, the density of the bismuth atom on both  $\Sigma 3$  and  $\Sigma 33$  boundary planes is 50 at. %. The equilibrium structures of both pure and Bi-segregated boundaries are obtained using a pseudodynamics method.<sup>20</sup> The procedure of the energy minimization only involves the local atomic relaxation, which terminates when the forces on all atoms fall below  $5 \times 10^{-4}$  eV  $\text{\AA}^{-1}$ .

During the simulation of deformation and fracture of the bicrystals, the external load is applied by imposing a relative strain in the  $X$  direction between each atom in region II and its inner nearest neighboring atom. This can be in region II or I, i.e., by keeping their distance at  $1 + \Delta$  of the corresponding distance in the original relaxed structure unloaded, where  $\Delta$  is chosen to be 0.07 in all the simulations. The atoms in region II are then allowed to move in the  $X$  direction. Except for the above loading constraint, all atomic positions in region I are free to adjust and be simulated by the MD method. The length of each time step is chosen to be 0.04 in a normalized time unit, i.e.,  $1.2 \times 10^{-14}$  s, which gives good precision in solving the Newton equations by the leap-frog algorithm.

### III. RESULTS AND DISCUSSION

#### A. Relaxed structures of the GBs

The relaxed structures of the pure  $\Sigma 3$  and  $\Sigma 33$  boundaries are shown in Figs. 3(a) and 3(b), where the triangle and cross represent atoms in two different adjacent (101) planes. The polyhedra occurring in the GBs associated with the structural units are pictured on the (101) plane. It can be seen that the  $\Sigma 3$  GB consists of one single type of atomic polyhedra, that is, octahedra. Its GB energy is very low, equal to  $29 \text{ mJ m}^{-1}$ . The  $\Sigma 33$  boundary is found to be composed of three structural units of the  $\Sigma 3$  GB and

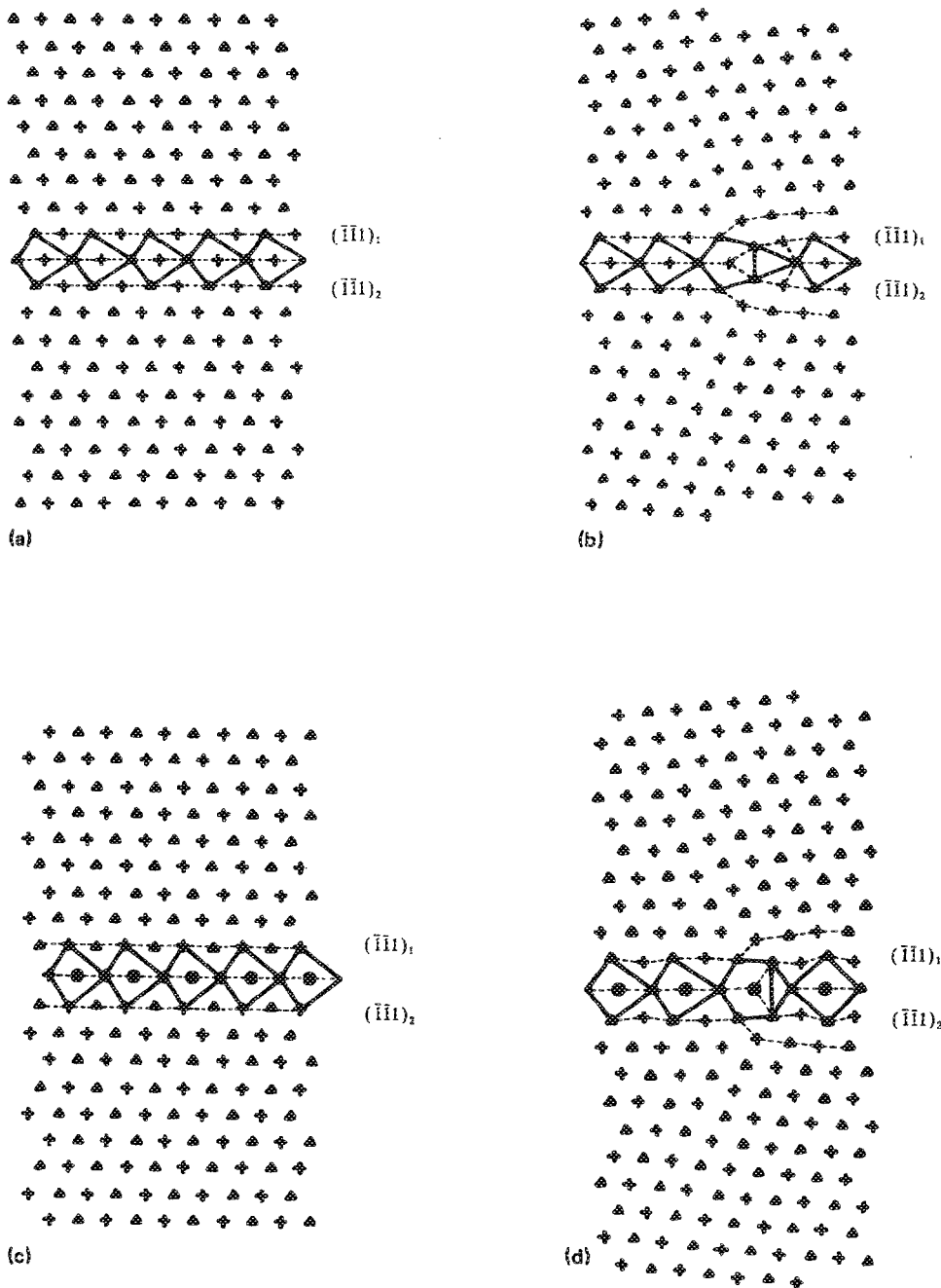


FIG. 3. The relaxed structures of grain boundaries (GBs): (a) the pure  $\Sigma 3$   $(\bar{1}\bar{1}1)/[101]$  tilt GB; (b)  $\Sigma 33$   $(\bar{5}\bar{4}5)/[101]$  tilt GB; (c) the Bi-segregated  $\Sigma 3$  GB; (d) the Bi-segregated  $\Sigma 33$  GB (where  $\blacktriangle$ ,  $+$  indicate the atom positions in two adjacent planes,  $(101)$  and  $(202)$ , respectively;  $\bullet$  indicates the Bi atom position).

one pentagonal bipyramid plus a capped trigonal prism, which corresponds to the structural unit of the  $\Sigma 9(2\bar{1}2)/[101]$  GB.<sup>16</sup> According to the structural unit model,<sup>21,22</sup> the intrinsic GB dislocation (GBD) of the  $\Sigma 33$  GB is located at the minority unit, i.e., the  $\Sigma 9$  GB unit. As shown in Fig. 3(b),  $(\bar{1}\bar{1}1)$  planes denoted by dashed lines terminate at this structural unit. The Burgers vector of the GBD in the  $\Sigma 33$  boundary is equal to  $2/3[\bar{1}\bar{1}1]$ . The energy of  $\Sigma 33$  GB is  $1185 \text{ mJ m}^{-1}$ .

The relaxed structures for the Bi-segregated  $\Sigma 3$  and  $\Sigma 33$  GBs are shown in Figs. 3(c) and 3(d), respectively, where full circles indicate the positions of Bi atoms at the vertexes of the polyhedra. The segregation of bismuth atoms is accompanied by expansion of the GB core in the direction perpendicular to the GB. In addition, the dis-

tances between the copper atoms on the fringe of the  $\Sigma 3$  structural units and their nearest neighbor copper atoms also expand. This result is similar to that obtained by Chang *et al.*<sup>17</sup> Sutton and Vitek<sup>18</sup> also found that the segregation of Bi atom in copper boundaries is accompanied by the expansion in the direction perpendicular to the boundaries, which was interpreted as weakening of boundary cohesion. In the present case, the expansion between the fringe Cu atoms and their neighboring Cu atoms also means the weakening of the chemical bonds between Cu—Cu atoms. While the expansion of the structural units does not mean the weakening of the chemical bonds within the structural units due to the strong binding force between the Bi atom and Cu atom, which is manifested by the Cu—Cu and Cu—Bi potential curves shown in Fig. 1. This

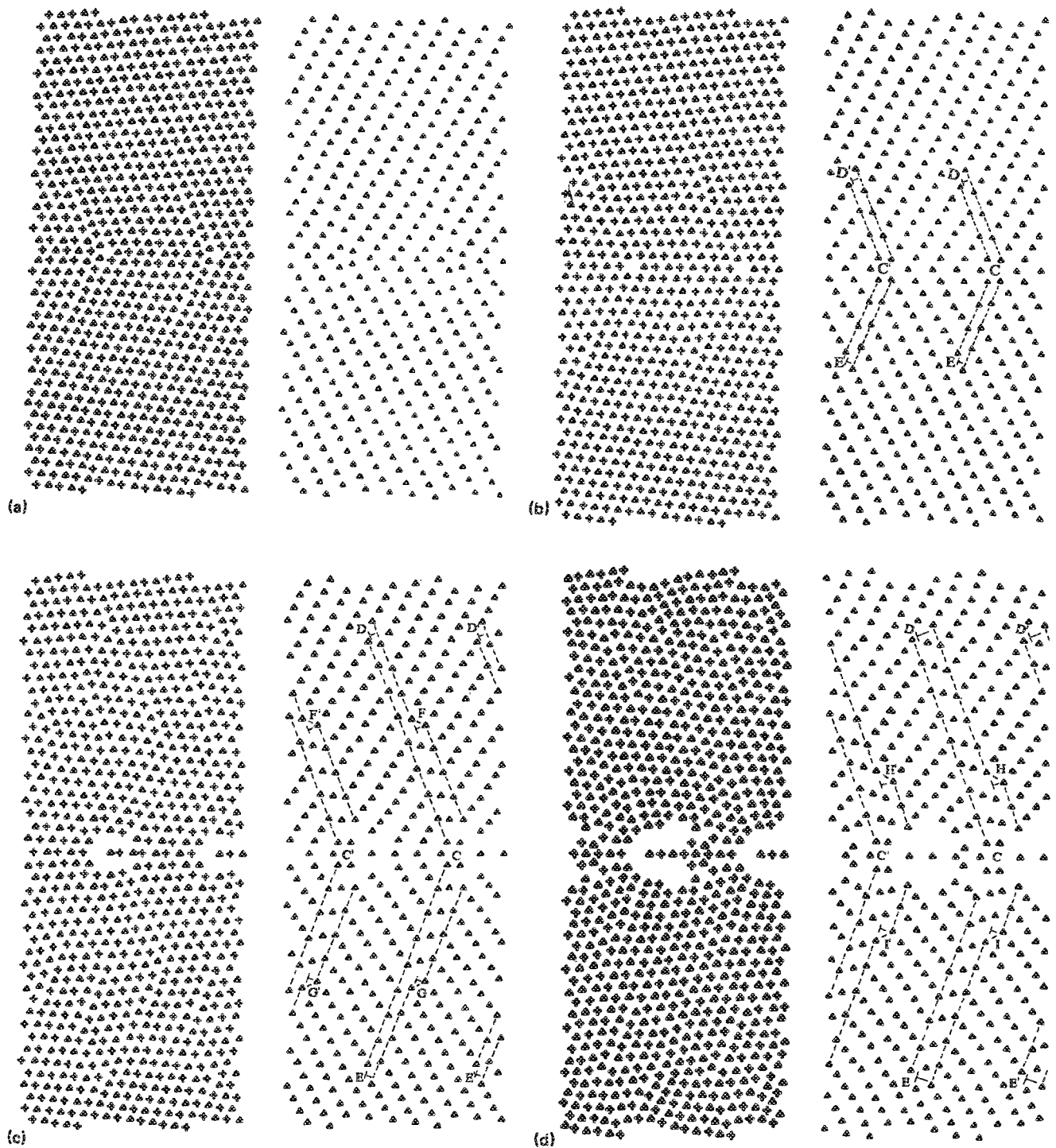


FIG. 4. The microprocess of deformation and fracture of copper bicrystal along the pure  $\Sigma$  33 GB [the right figure of each time step is the corresponding atom positions in the (101) plane]. Time steps (a) 15; (b) 90; (c) 165; (d) 210; (e) 250; and (f) 300.

result is consistent with the study of the electron charge transfer between copper atoms and bismuth atoms in the GB of metal copper induced by bismuth segregation.<sup>7</sup> Larger relaxation happens at the site of the GBD than at the other area of  $\Sigma$  33 GB. This indicates that the large bismuth atom is more able to segregate at this site. The change of the GB energy induced by the segregation of per bismuth atom in  $\Sigma$  3 and  $\Sigma$  33 GBs is 5.6 and 2.1 eV, respectively. This result indicates that the bismuth atom is difficult to segregate at  $\Sigma$  3 GB, but easy to segregate at  $\Sigma$  33 GB.

## B. Microprocess of deformation and fracture

### 1. The pure $\Sigma$ 33 tilt bicrystal

The microprocess of deformation and fracture for the pure  $\Sigma$  33 bicrystal is shown in Fig. 4, where two periods of the computational cell in the Y direction are plotted. To be more distinct, the atoms in a single (101) plane are also shown on the left of the figure for the corresponding time step. For the time step less than 50, only elastic deformation occurs, with no dislocation created in the two grains,

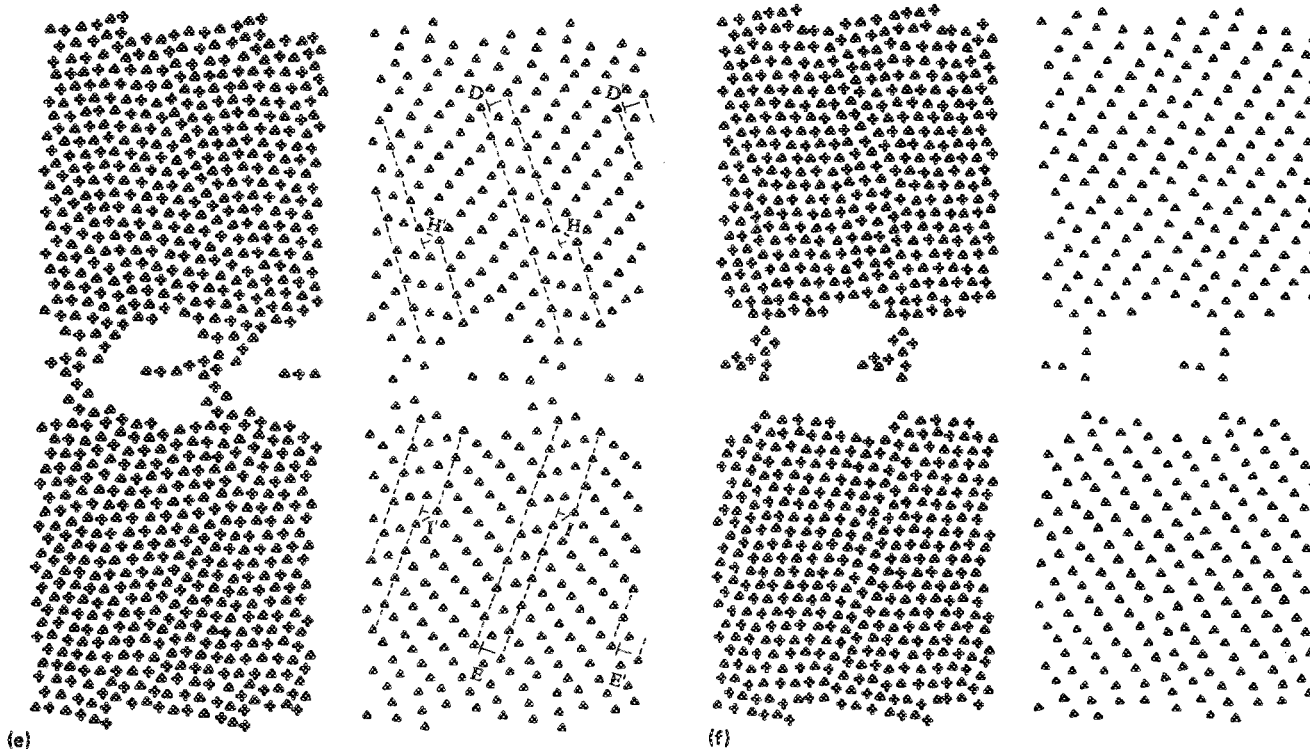


FIG. 4. (Continued).

as shown in Fig. 4(a). Afterward, Shockley partial dislocations with Burgers vector equal to  $1/4[\bar{1}21]$  are created at the GBDs and glide along the  $[\bar{1}21]$  direction as shown by D and E in Fig. 4(b). Following the glide of the partial dislocations in the grains, twinning bands are formed in the regions CD and CE as denoted by dashed lines, with stacking faults of the  $(\bar{1}11)$  planes represented by ...ABCAB. ABCAB...

In the process of partial dislocation generation and emission, vacancies are created and embryos of voids are formed. As strain increases, new partial dislocations are produced and glide on other  $(\bar{1}11)$  planes, as marked by F and G in Fig. 4(c) and by H and I in Fig. 4(d). Hence, the twinning bands become larger and wider. More vacancy generation leads to coalescence of voids, and finally results in ductile fracture.

## 2. The Bi-segregated $\Sigma 33$ tilt bicrystal

The microprocess of deformation and fracture for the segregated  $\Sigma 33$  bicrystal is shown in Fig. 5. In the early stage of deformation, Shockley partial dislocations with Burgers vector equal to  $1/4[\bar{1}21]$  are generated from the GBDs of the  $\Sigma 9$  GB units and glide on the  $(\bar{1}11)$  planes, as denoted by solid lines in Fig. 5(a). Segregation of Bi atoms weakens the atomic bonds between the copper atoms in the vicinity of the GB, as discussed in Sec. III A. Hence microcracks nucleate along the  $\Sigma 3$  units, caused by the breaking of the weakened Cu—Cu bonds, as shown in Figs. 5(b) and 5(c). This corresponds to the brittle intergranular fracture.

## 3. The pure $\Sigma 3$ tilt bicrystal

The microprocess of deformation and fracture for the pure  $\Sigma 3$  bicrystal is shown in Fig. 6. Since the  $\Sigma 3$  GB is a coherent twin boundary with no GBD, no dislocation is generated in the grains before the time step 200. The large stress concentration at the GB gradually causes a large local distortion and Shockley partial dislocations with Burgers vectors equal to  $1/6[\bar{1}21]$  are emitted from those distorted regions, as indicated by the lines in Fig. 6(a). The lattice distortion leads to formation of vacancies and voids, as shown in Fig. 6(b) and 6(c), and the void coalescence results finally in ductile fracture, as shown in Fig. 6(d).

## 4. The Bi-segregated $\Sigma 3$ tilt bicrystal

The microprocess of deformation and fracture for the segregated  $\Sigma 3$  bicrystal is shown in Fig. 7, where only one period of the computational cell in the  $Y$  direction is plotted. Under the external load, the segregated  $\Sigma 3$  bi-crystal is more brittle. Fracture also proceeds by means of breaking of weakened Cu—Cu bonds between the structural units and surrounding atoms. In the grains no dislocation generates. Only lattice distortion near the fracture surfaces is observed.

## IV. CONCLUSIONS

The above results indicate that the microprocess of deformation and fracture for copper bicrystals is dependent on the grain boundary structure and bismuth segregation.

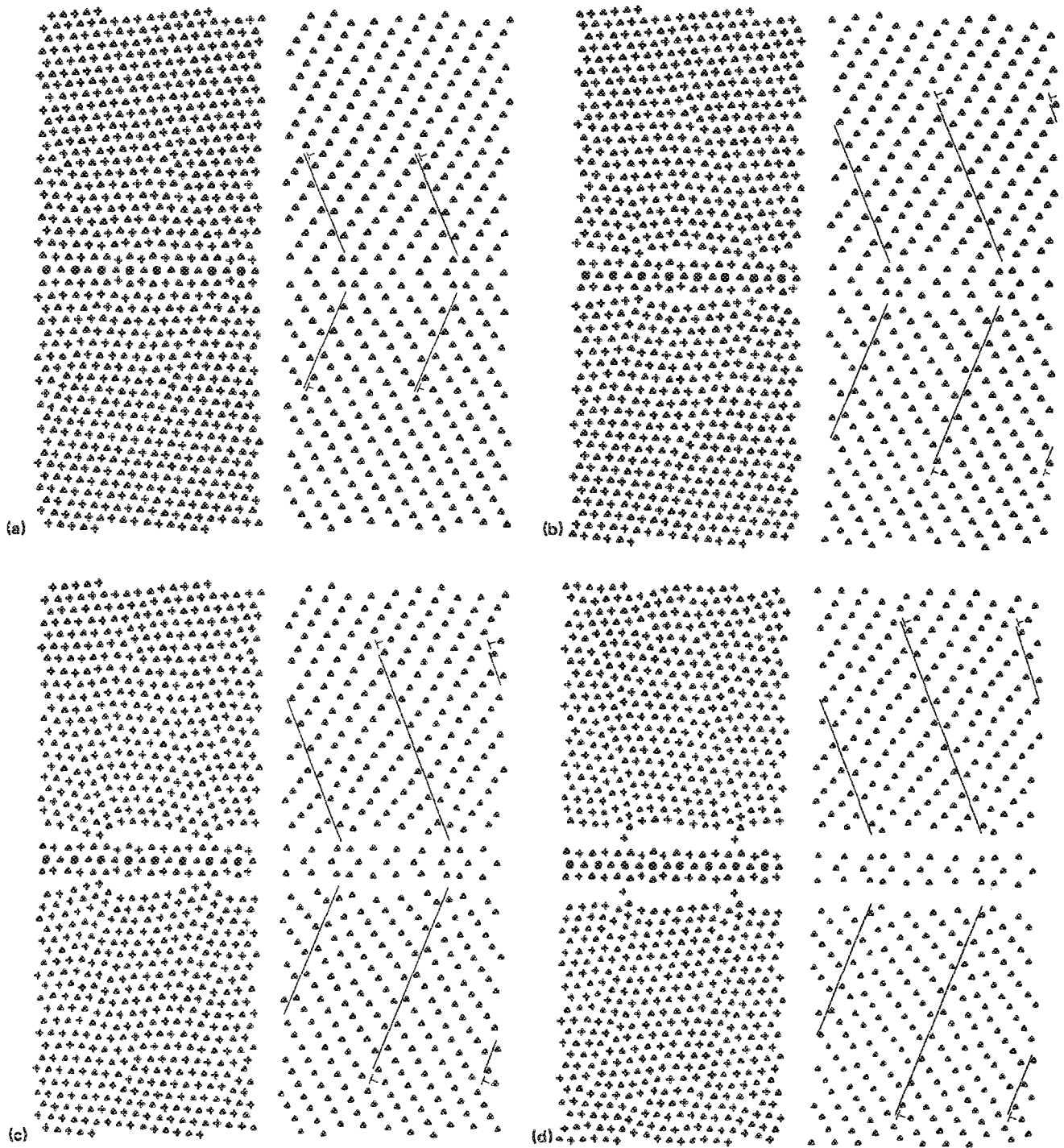


FIG. 5. The microprocess of deformation and brittle fracture along the Bi-segregated  $\Sigma$  33 GB. Time steps: (a) 96; (b) 128; (c) 152; and (d) 184.

(A) For copper bicrystal with  $\Sigma$  33 tilt boundary, the deformation is mainly due to the generation and glide of partial dislocations, initiated from the structural units where GB dislocation exists. The ductile fracture is caused by the dislocation emission which leads to the vacancy generation and void coalescence. Bismuth segregation weakens the atomic bonds between copper atoms in the vicinity of the GB. Under the action of the external load,

the weakened Cu—Cu bonds break. The broken bonds lead to the formation of microcracks and finally result in brittle fracture.

(B) For the case of the tilt bicrystal containing low coherent boundary,  $\Sigma$  3 GB, dislocation generation and emission are mainly due to the lattice distortion caused by the external load. The brittle fracture induced by bismuth segregation is also controlled by the presence of weakened

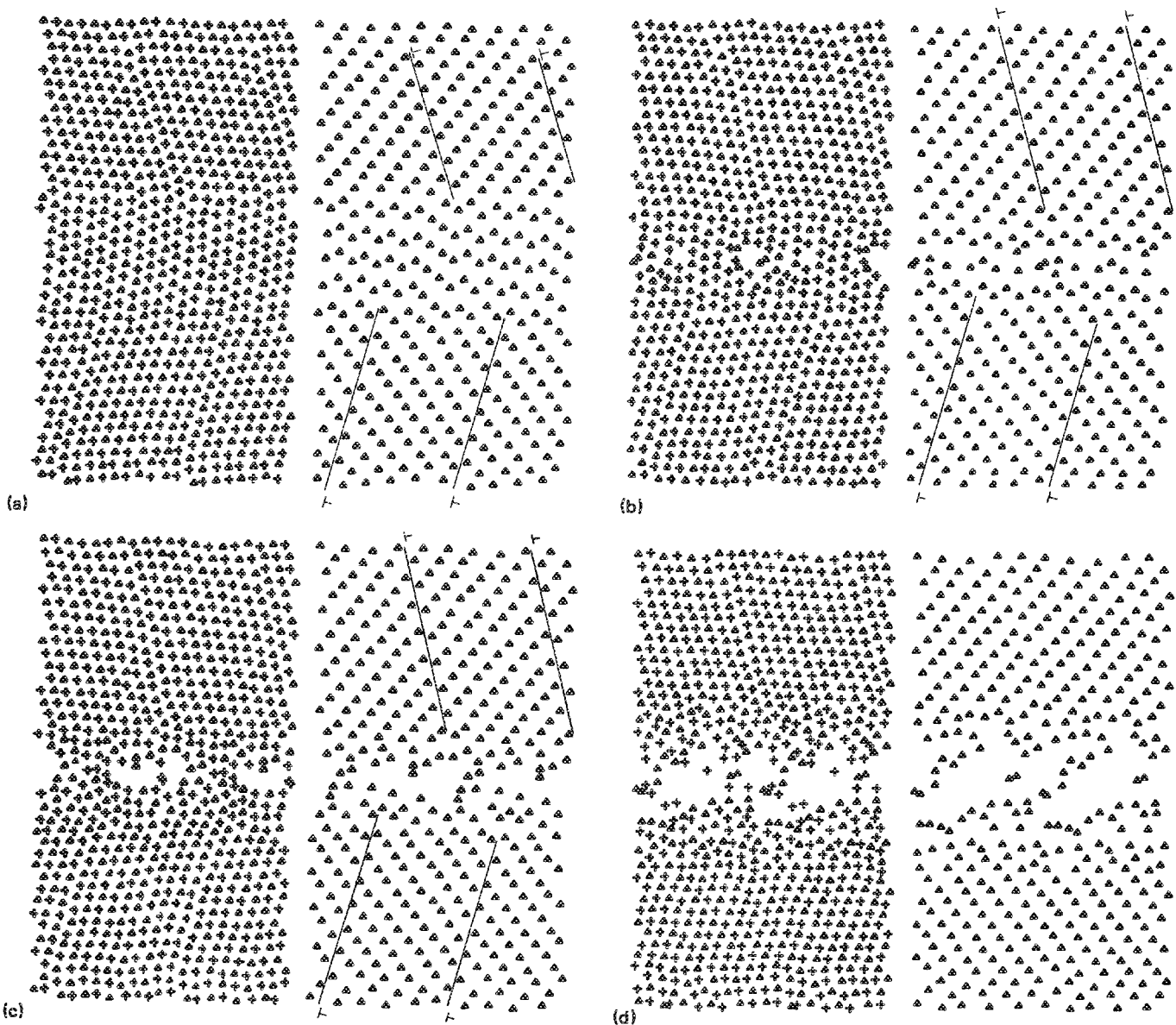


FIG. 6. The microprocess of deformation and fracture of copper bicrystal along the pure  $\Sigma$  33 GB. Time steps (a) 471; (b) 511; (c) 521; and (d) 551.

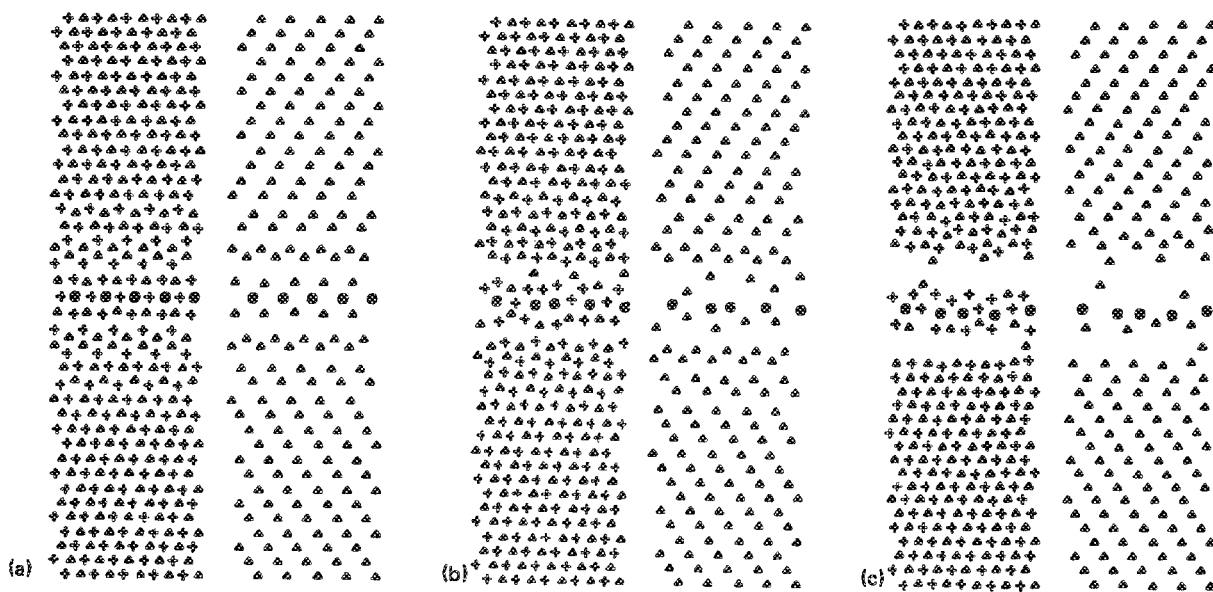


FIG. 7. The microprocess of deformation and fracture along the Bi-segregated  $\Sigma$  3 GB. Time steps: (a) 150; (b) 168; and (c) 204.

## ACKNOWLEDGMENTS

One of the authors X.J.W. would like to thank Professor C. W. Lung from the Institute of Metal Research, Chinese Academia of Science (CAS), Shenyang, China, and Professor R. Thomson from the National Institute of Standards and Technology, Washington, DC, during the Working Party on Fracture Physics at the International Center for Theoretical Physics (ICTP), Trieste, Italy, 29 May–16 June, 1989. The work was supported by CAS under grant No. 87-52, and by the Laboratory for Nonlinear Mechanics of Continuous Media (LNM), Institute of Mechanics, CAS.

- <sup>1</sup>E. Voce and A. P. C. Hallows, *J. Inst. Met.* **73**, 323 (1947).
- <sup>2</sup>E. D. Hondros and D. McLean, *Philos. Mag.* **29**, 771 (1974).
- <sup>3</sup>E. D. Hondros and M. P. Seah, in *Physical Metallurgy*, 3rd ed., edited by R. W. Cahn and P. Hassen (Elsevier, New York, 1983), p. 586.
- <sup>4</sup>J. R. Russel and A. T. Winter, *Scr. Metall.* **19**, 575 (1985).
- <sup>5</sup>S. Chikwembani and J. Weertman, *Scr. Metall.* **19**, 1499 (1985).

- <sup>7</sup>Q. Qui, X. J. Wu, G. H. Li, M. Cai, Q. H. Tang, and X. Y. Qin (unpublished).
- <sup>8</sup>X. J. Wu, Q. Q. Zheng, B. Hu, Z. Zeng, F. X. Zhou, and Z. Y. Chen, *Proceedings of the 3rd International Conference on the Strength of Metals and Alloys, Tampere, Finland* (Pergamon, New York, 1988), p. 1369.
- <sup>9</sup>H. K. Chang, R. S. Weidman, and J. K. Lee, *Surf. Sci.* **144**, 224 (1984).
- <sup>10</sup>Y. Ishida, M. Mori, and M. Hashimoto, *Surf. Sci.* **144**, 253 (1984).
- <sup>11</sup>M. I. Baskes, S. M. Foiles, and M. S. Daw, *J. Phys. (Paris)* **49**, C5–483 (1988).
- <sup>12</sup>M. S. Daw and M. I. Baskes, *Phys. Rev. B* **29**, 6443 (1984).
- <sup>13</sup>M. S. Daw, *Phys. Rev. B* **39**, 7441 (1989).
- <sup>14</sup>M. W. Finnis and J. E. Sinclair, *Philos. Mag. A* **50**, 45 (1984).
- <sup>15</sup>G. J. Ackland, G. Tichy, V. Vitek, and M. W. Finnis, *Philos. Mag. A* **56**, 735 (1987).
- <sup>16</sup>K. Maeda, V. Vitek, and A. P. Sutton, *Acta Metall.* **30**, 2001 (1982).
- <sup>17</sup>B. Y. Peng (unpublished).
- <sup>18</sup>H. K. Chang, J. K. Lee, and D. F. Stein, in *Interatomic Potentials and Crystalline Defects*, edited by J. K. Lee (TMS-AIME, Warrendale, PA, 1981), p. 373.
- <sup>19</sup>A. P. Sutton and V. Vitek, *Acta Metall.* **30**, 2011 (1982).
- <sup>20</sup>R. C. Pond, V. Vitek, and D. A. Smith, *Acta Cryst. A* **35**, 689 (1979).
- <sup>21</sup>R. E. Dahl, T. R. Beeler, and R. D. Burguin, *Comput. Phys. Commun.* **2**, 301 (1970).
- <sup>22</sup>A. P. Sutton and V. Vitek, *Scr. Metall.* **14**, 129 (1980).
- <sup>23</sup>A. P. Sutton and V. Vitek, *Philos. Trans. R. Soc. London A* **309**, 1 (1983).